

# Time evolution of rotating and magnetized white dwarf stars

L. Becerra,<sup>1,2\*</sup> K. Boshkayev,<sup>3,4†</sup> J. A. Rueda<sup>1,2,5‡</sup> and R. Ruffini<sup>1,2,5§</sup>

<sup>1</sup>ICRANet, Piazza della Repubblica 10, I-65122 Pescara, Italy

<sup>2</sup>Dipartimento di Fisica and ICRA, Sapienza Università di Roma, P.le Aldo Moro 5, I-00185 Rome, Italy

<sup>3</sup>NNLOT, al-Farabi Kazakh National University, Al-Farabi av. 71, 050040 Almaty, Kazakhstan

<sup>4</sup>Department of Physics, Nazarbayev University, Kabanbay Batyr 53, Astana 010000, Kazakhstan

<sup>5</sup>ICRANet-Rio, CBPF, Rua Dr. Xavier Sigaud 150, Rio de Janeiro, RJ, 22290–180, Brazil

26 November 2021

## ABSTRACT

We investigate the evolution of isolated, zero and finite temperature, massive, uniformly rotating and highly magnetized white dwarf stars under angular momentum loss driven by magnetic dipole braking. We consider the structure and thermal evolution of the white dwarf isothermal core taking also into account the nuclear burning and neutrino emission processes. We estimate the white dwarf lifetime before it reaches the condition either for a type Ia supernova explosion or for the gravitational collapse to a neutron star. We analyze the behavior of the WD parameters such as the central density, radius, moment of inertia, angular momentum, angular velocity, central temperature and magnetic field intensity as a function of lifetime. In addition, we compute the characteristic time of nuclear reactions and dynamical time scale. The astrophysical consequences of the results are discussed.

## 1 INTRODUCTION

In this work we investigate the time evolution of massive, uniformly rotating, highly magnetized white dwarfs (WDs) when they lose angular momentum owing to magnetic dipole braking. We have different important reasons to perform such an investigation: 1) there is incontestable observational data on the existence of massive ( $M \sim 1 M_{\odot}$ ) WDs with magnetic fields all the way to  $10^9$  G (see (Kepler et al. 2015), and references therein); 2) WDs can rotate with periods as short as  $P \approx 0.5$  s (Boshkayev et al. 2013b); 3) they can be formed in double WD mergers (García-Berro et al. 2012; Rueda et al. 2013; Kilic et al. 2018); 4) they have been invoked to explain type Ia supernovae within the *double degenerate scenario* (Webbink 1984; Iben & Tutukov 1984); 5) they constitute a viable model to explain soft gamma-repeaters and anomalous X-ray pulsars (Malheiro et al. 2012; Boshkayev et al. 2013a; Rueda et al. 2013; Boshkayev et al. 2015a).

Thus, it is of astrophysical importance to determine qualitatively and quantitatively the evolution of micro and macro physical properties such as density, pressure, temperature, mass, radius, moment of inertia, and angular velocity/rotation period of massive, uniformly rotating, highly magnetized WDs. We constrain ourselves in this work to study the specific case when the WD is isolated and it is losing angular momentum via magnetic dipole braking.

Depending on their mass, WDs can exhibit different timing properties by losing angular momentum: uniformly and differentially rotating super-Chandrasekhar WDs (hereafter SCWDs) spin-up, whereas sub-Chandrasekhar WDs spin-down. The possibility that a rotating star spin-up by angular momentum loss was first revealed by Shapiro et al. (1990), and later by Geroyannis & Paspotiriou (2000). In both articles the WDs were studied within the Newtonian framework, though the effects of general relativity are crucial to determine the stability of massive, fast rotating

WDs (see, e.g., (Shapiro & Teukolsky 1983; Rotondo et al. 2011b; Boshkayev et al. 2013b, 2015b)). Besides the above timing features, we shall quantify the compression that the WD suffers while evolving via angular momentum loss which is relevant for some models of type Ia supernovae. Specifically, we focus on the compression of isolated zero-temperature super-Chandrasekhar WDs and their isothermal cores by angular momentum loss based on our previous results (Boshkayev et al. 2013b, 2014a,b, 2017). We shall estimate the lifetime ( $\tau$ ) of zero temperature WDs via magnetic dipole braking taking into due account the effect of the time evolution of all relevant parameters of the WDs. In addition, for hot isothermal WD cores we compute the times of the nuclear burning and neutrino emission phenomena. For both cold and hot WDs, we consider two magnetic field evolution: (1) a constant magnetic field during the entire evolution and, (2) a varying magnetic field according to magnetic flux conservation.

Our paper is organized as follows: in section 2, we discuss about WD equation of state, stability conditions and spin-up and spin-down effects; in section 3 we estimate the lifetime of SCWDs; in section 4 we show the compression of the WD during its evolution; and in section 5 we consider the central temperature evolution for isothermal WD cores. Finally, we summarize our results in section 6, discuss their significance, and draw our conclusions.

## 2 WD EQUATION OF STATE AND STABILITY

We follow in this work the treatment of Boshkayev et al. (2013b). We compute general relativistic configurations of uniformly rotating WDs within Hartle’s formalism (Hartle 1967; Boshkayev et al. 2011) and use the relativistic Feynman-Metropolis-Teller equation of state (Rotondo et al. 2011b,a) for WD matter. This equation of state generalizes the traditionally-used ones by Chandrasekhar (1931) and Salpeter (1961) in the following aspects: (1) it insures

arXiv:1812.10543v1 [astro-ph.SR] 26 Dec 2018

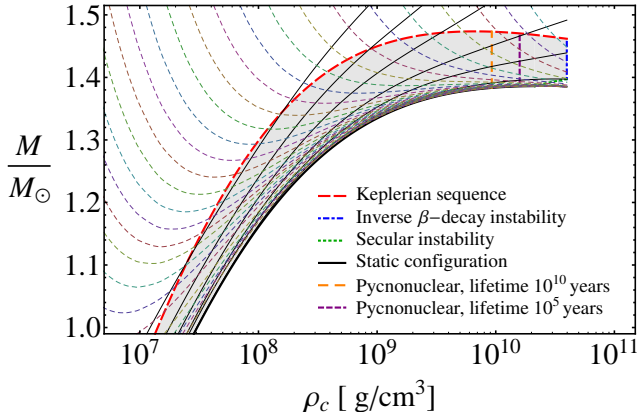


**Figure 1.** (Color online) Total mass versus central density of rotating  $^{12}\text{C}$  WDs. The solid black curves are angular momentum  $J=\text{constant}$  sequences, where the static case  $J = 0$  is the thickest black curve. The colored thin-dashed curves are angular velocity  $\Omega=\text{constant}$  sequences. The mass-shedding limit is the red thick-dashed curve, the blue thick-dotted-dashed curve is the inverse  $\beta$ -decay instability line, and the green-thick dotted curve is the axisymmetric secular instability border. The gray-shaded region is the stability region of uniformly rotating white dwarfs.

self-consistency of a relativistic treatment of the electrons by introducing a finite-sized nucleus; (2) the Coulomb energy is found from the numerical solution of the relativistic Thomas-Fermi equation; (3) the same applies to the inhomogeneity of the electron distribution inside each Wigner-Seitz cell; (4) the energy density of the system is estimated accounting for the contributions of the nuclei, the Coulomb interactions and the relativistic electrons to the energy of the Wigner-Seitz cells; and (5) the  $\beta$  equilibrium among neutrons and protons inside nuclei, and electrons is also considered, which leads to a self-consistent assess of the inverse  $\beta$  decay energy threshold. A detailed description of this equation of state and the differences with respect to other treatments are given by [Rotondo et al. \(2011b\)](#).

The stability of uniformly rotating WDs has been analyzed taking into account the Keplerian sequence (mass-shedding limit), inverse  $\beta$ -decay instability, and secular axisymmetric instability ([Boshkayev et al. 2013b](#)). We illustrate in Fig. 1 the mass-central density diagram of rotating WDs composed of pure  $^{12}\text{C}$  for various angular momentum  $J=\text{constant}$  and angular velocity  $\Omega=\text{constant}$  sequences. In addition, we have included the critical density for pycnonuclear instability (in this case C+C reaction at zero temperature) with reaction time scales  $10^5$  and  $10^{10}$  years. We suggest the reader ([Boshkayev et al. 2013b](#)) for additional details.

In Fig. 2, we show contours of constant rest-mass in the  $\Omega - J$  plane which will be used in the next section. All curves inside the stability region correspond to the fixed rest-mass sequence. Rotating WDs that evolve along a track with  $\partial\Omega/\partial J > 0$  spin-down by losing angular momentum while the ones with  $\partial\Omega/\partial J < 0$  spin-up by (see ([Boshkayev et al. 2013b](#)) for details).

### 3 SUPER-CHANDRASEKHAR WD LIFETIME

We are interested in estimating the evolution of magnetized WDs when they are losing angular momentum via the magnetic dipole braking. It is well known that this braking mechanism needs, for

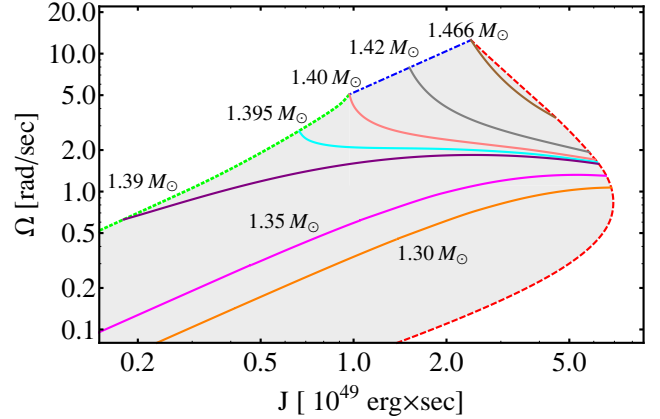


**Figure 2.** (Color online) Contours of constant rest-mass in the  $\Omega - J$  plane. The mass-shedding limit is the red thick-dashed curve, the blue thick-dotted-dashed curve is the inverse  $\beta$ -decay instability line, and the green-thick dotted curve is the axisymmetric secular instability border. The gray-shaded region is the stability region of rotating white dwarfs.

a rotating magnetic dipole in vacuum, that the magnetic field is misaligned with the rotation axis. It has been shown that such WD with misaligned fields could be formed in the merger of double degenerate binaries, and the degree of misalignment depends on the difference between the masses of the WD components of the binary ([García-Berro et al. 2012](#)).

Particularly interesting are the SCWDs which are stable by virtue of their angular momentum. Thus, by loosing angular momentum, they will evolve toward one of the aforementioned instability borders. This is the reason why, for example, magnetic braking of SCWDs has been invoked as a possible mechanism to explain the delayed time distribution of type Ia supernovae ([Ilkov & Soker 2012](#)): a type Ia supernova can be delayed for a time typical of the spin-down time scale  $\tau$  due to magnetic braking, providing the result of the merging process of a WD binary system is a magnetic SCWD rather than a sub-Chandrasekhar one. It is important to recall that in such a model it is implicitly assumed that the fate of the WD is a supernova explosion instead of gravitational collapse. The competition between these two possibilities is an important issue which deserves to be further analyzed but it is out of the scope of this work.

Since SCWDs spin-up by angular momentum loss the reference to a “spin-down” time scale for them can be misleading. Thus, we prefer hereafter to refer the time the WD spend in reaching an instability border (either mass-shedding, secular or inverse  $\beta$  instability; see Fig. 1, where we show  $\Omega =\text{constant}$  and  $J =\text{constant}$  sequences in the mass-central density diagram, and in Fig. 2, we show contours of constant rest-mass in the  $\Omega - J$  plane.) as the WD lifetime,  $\tau$ .

As we have shown, the evolution track followed by a SCWD depends strongly on the initial conditions of mass and angular momentum, as well as on the nuclear (chemical) composition and the evolution of the moment of inertia. Clearly, the assumption of fixed moment of inertia leads to a lifetime scale that depends only on the magnetic field’s strength. A detailed computation will lead to a strong dependence on the mass of the SCWD, resulting in a two-parameter family of lifetime  $\tau = \tau(M, B)$ . Indeed, we see from Fig. 3 that the moment of inertia even for a static case is not constant since it is a function of the central density. In the rotating case

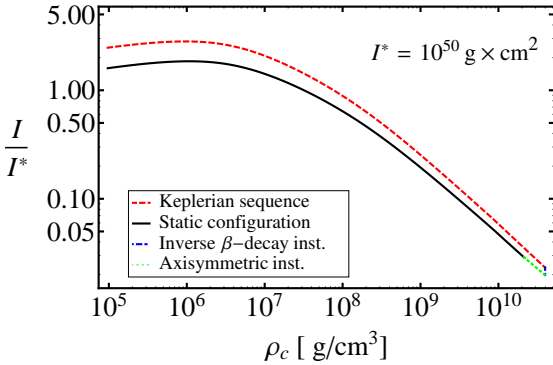


**Figure 3.** Moment of inertia versus central density.

it is a function of both central density and angular velocity (rotation period).

Thus, we have estimated the characteristic lifetime relaxing the constancy of the moment of inertia, radius and other parameters of rotating WDs. In fact we show here that all WD parameters are functions of the central density and the angular velocity. We used the lifetime formula preliminary expressing it in terms of the mean radius  $\langle R \rangle \equiv (1/3)(R_{\text{polar}} + 2R_{\text{equatorial}})$  and the angular velocity  $\Omega$  as a function of the central density  $\rho$  and the angular momentum  $J$  for practical purposes:

$$\begin{aligned} \langle R \rangle &= \langle R \rangle(\rho, J), \quad \Omega = \Omega(\rho, J), \\ \tau(M, B) &= -\frac{3c^3}{2B^2} \int_{J_{\text{max}}}^{J_{\text{min}}} \frac{1}{\langle R \rangle^6 \Omega^3} dJ, \end{aligned} \quad (1)$$

though the original form of the above equation is given by

$$dt = -\frac{3}{2} \frac{c^3}{B^2} \frac{1}{\langle R \rangle^6} \frac{1}{\Omega^3} dJ, \quad (2)$$

where  $c$  is the speed of light,  $B$  is the magnetic field intensity in Gauss, and  $J$ ,  $\Omega$  and  $\langle R \rangle$  are calculated along the specific constant-rest-mass sequences shown in Fig. 2. Hence, we performed more refined analyzes with respect to Ilkov & Soker (2012) by taking into consideration all the stability criteria, with the only exception of the instabilities related to nuclear reactions (either pynuclear or enhanced by finite temperature effects) which we will consider in Sec. 5.

The characteristic lifetime  $\tau$  as a function of WD mass in units of  $M_{\text{max}}^{J=0}$  for zero temperature uniformly rotating  $^{12}\text{C}$  WDs is depicted on the left panel of Fig. 4. One can see that the higher the magnetic field, the shorter the lifetime of the rotating SCWD. Correspondingly, a more massive WD will have a shorter life span and vice versa.

Moreover, one can see how for a fixed magnetic field value, the lifetime has a wide range of values as a function of the mass, being inversely proportional to the latter. The time scales of Ilkov & Soker (2012); Külebi et al. (2013) appear to be consistent with the ones in Fig. 4 only for the maximum mass value  $M/M_{\text{max}}^{J=0} \approx 1.06$ . Another interesting representation of life time is demonstrated on the right panel of Fig. 4, where the characteristic lifetime is plotted versus the surface magnetic field for given sets of constant mass sequences (Boshkayev et al. 2014b). Here each straight line corresponds to a certain fixed constant mass sequence. By choosing one value or the whole range of the magnetic field intensity one can estimate the lifespan of a SCWD for a given mass.

#### 4 INDUCED COMPRESSION

To investigate the evolution of isolated white dwarfs with time we made use of Eq. (2) and modified it depending on what parameter we are interested in (see (Boshkayev et al. 2017) for details).

We adopt two cases: 1) when the magnetic field is constant and 2) when magnetic flux is conserved

$$B = B_0, \quad (3)$$

$$B = B_0 \frac{\langle R_0 \rangle^2}{\langle R \rangle^2}, \quad (4)$$

where  $B_0$  is the surface dipole magnetic field corresponding to the initial value of  $B$  at  $t = 0$ ,  $\langle R_0 \rangle$  is the mean radius corresponding to the initial values of  $\langle R \rangle$  at  $t = 0$ . Plugging  $B$  in Eq. (2) we obtain two separate equations that describe the evolution of a considered parameter with time taking into account two cases when magnetic field is constant and when magnetic flux is conserved. On the left panel of Fig. 5 we can see the main difference between two cases. In both cases WDs will increase their central density and will be compressed by losing angular momentum. Nonetheless in the case with the magnetic flux conservation the value of  $B$  will be increasing due to the compression thus causing more torque and evolving faster with respect to the constant magnetic field case.

On the right panel of Fig. 5 the mean radius is plotted as a function of time, where solid curves indicate the evolution path when the magnetic field is constant and dashed curves indicate the evolution path when the magnetic flux is conserved with  $B_0 = 10^6$  G for selected constant mass sequences. Over the course of time the mean radius decreases, hence WDs shrink with time. For the case of the conserved magnetic flux it decreases faster than for the case with constant surface magnetic field.

For isolated rotating white dwarfs the rest mass remains unchanged in their entire evolution time and hence we see a direct correlation between the mean radius and the moment of inertia of WDs from Figs. 5 (right panel) and 6 (left panel).

On the right panel of Fig. 6 we plot angular velocity of WDs as a function of time, where the description of the curves is the same as in Fig. 5. Here one can see that for mass  $1.39M_{\odot}$  the WD spins-up at the beginning and spins-down at the end, whereas super-Chandrasekhar WDs spin-up only. This is another confirmation of our previous calculations (see e.g. Fig. 2). Since the angular momentum is lost by magnetic dipole braking in Fig. 7 (left panel) we see for larger masses it decreases even faster than for smaller masses.

The right panel of Fig. 7 describes how the surface magnetic field changes with time in the case of a conserved magnetic flux, for selected constant rest mass sequences. The magnetic field  $B$  increases as a result of the WD compression. This implies that at a certain point of their evolution WDs with “smaller” masses, but still with super-Chandrasekhar value, can attain high magnetic fields.

Overall, as one can see from the plots above the isolated WDs regardless of their masses due to magnetic dipole braking will always lose angular momentum (see e.g. Fig. 7 (left panel)). Therefore WDs will tend to reach a more stable configuration by increasing their central density and by decreasing their mean radius (see e.g. Fig. 5). Ultimately, super-Chandrasekhar WDs will spin-up and sub-Chandrasekhar WDs spin-down. As for the WDs having masses near the Chandrasekhar mass limit, they will experience both spin up and spin down epochs at certain time of their evolution and Fig. 6 (right panel) is another nice visual representation of these epochs.

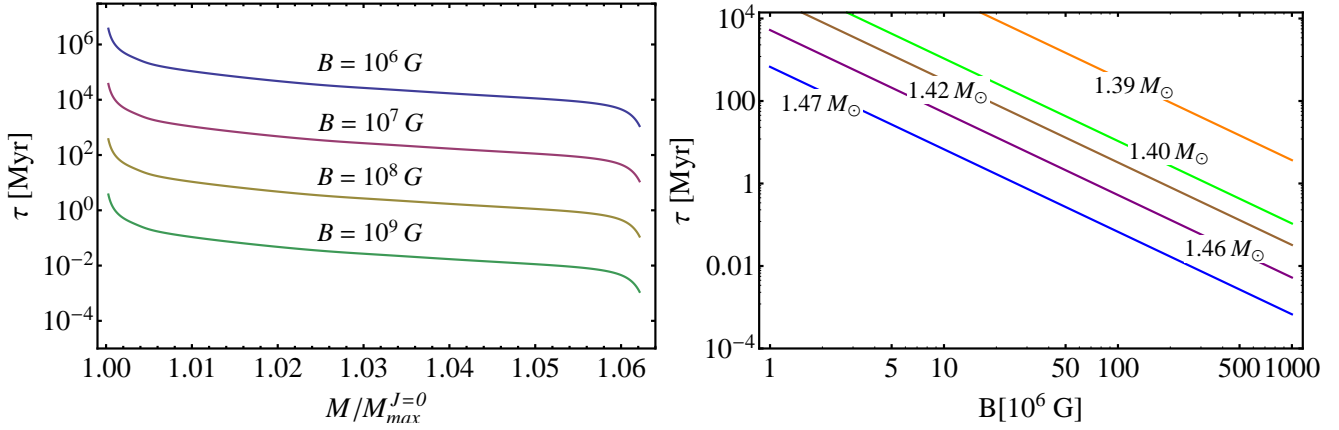


**Figure 4.** (Color online) Left panel: Characteristic lifetime  $\tau$  in Myr versus WD mass in units of  $M_{max}^{J=0} = 1.389 M_{\odot}$ . Right panel: Characteristic life time  $\tau$  in Myr versus WD surface magnetic field  $B$  in Gauss for rotating  $^{12}\text{C}$  WDs.

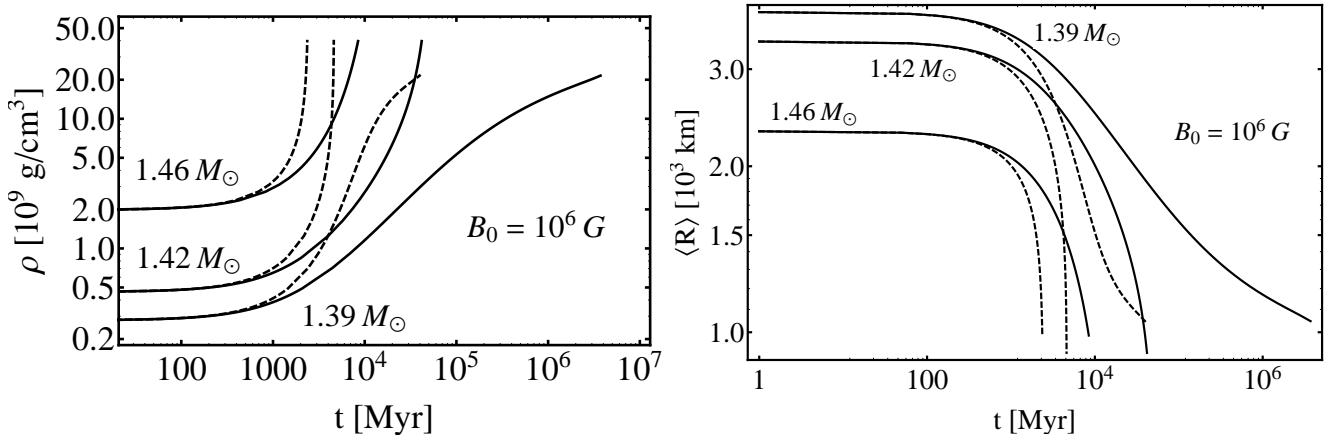


**Figure 5.** Left panel: Central density versus time. Right panel: Mean radius versus time. For both panels the solid curves indicate the evolution path when the magnetic field is constant and dashed curves indicate the evolution path when the magnetic flux is conserved with  $B_0 = 10^6$  G for selected constant mass sequences.

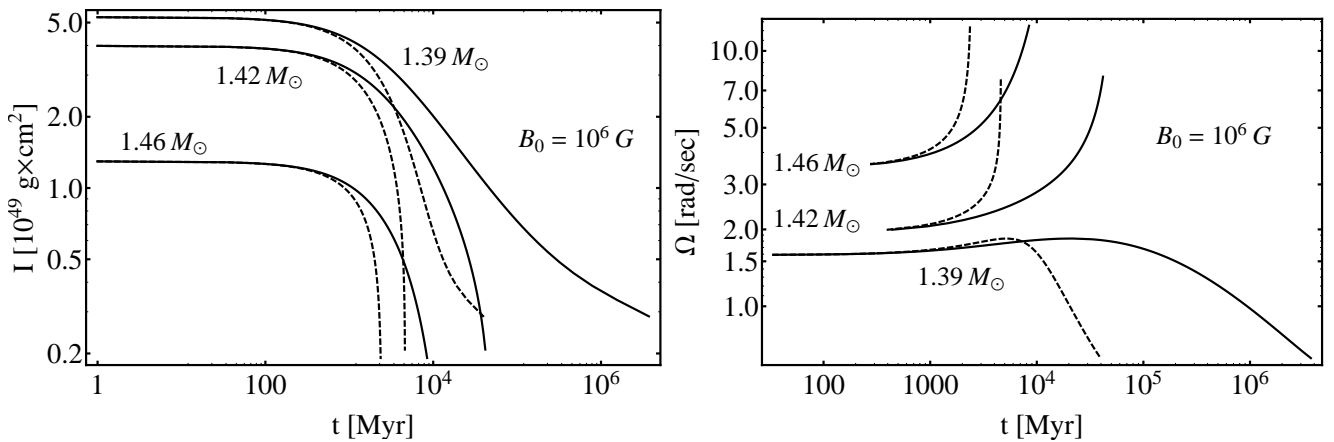


**Figure 6.** Left panel: Moment of inertia versus time. Right panel: Angular velocity versus time. For both panels the solid curves indicate the evolution path when the magnetic field is constant and dashed curves indicate the evolution path when the magnetic flux is conserved with  $B_0 = 10^6$  G for selected constant mass sequences.

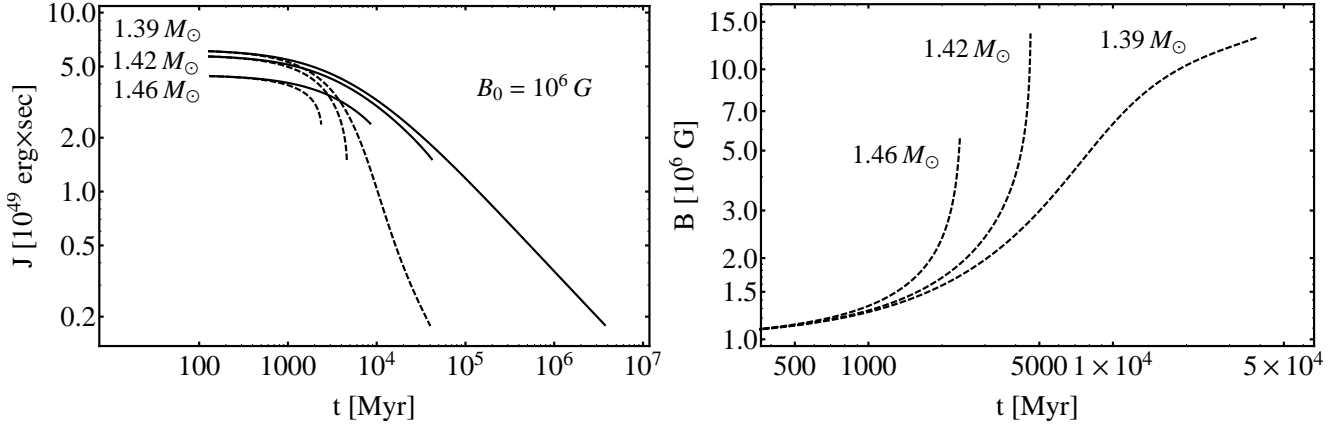


**Figure 7.** Left panel: Angular momentum versus time. Solid curves indicate the evolution path when the magnetic field is constant and dashed curves indicate the evolution path when the magnetic flux is conserved with  $B_0 = 10^6$  G for selected constant mass sequences. Right panel: Magnetic field versus time. The magnetic field is calculated only in case of the magnetic flux conservation.

## 5 CENTRAL TEMPERATURE EVOLUTION

In this section, we will model a SCWD as an isothermal core and follow its thermal evolution by solving the equation of energy conservation:

$$\frac{dL}{dm} = \epsilon_{\text{nuc}} - \epsilon_{\nu} + T\dot{s} \quad (5)$$

where  $L$  is the luminosity,  $\epsilon_{\text{nuc}}$  is the nuclear reactions energy release per unit mass,  $\epsilon_{\nu}$  is the energy loss per unit mass by the emission of neutrinos,  $T$  is the temperature and  $s$  is the specific entropy. The last term of Eq. (5) can be written as:

$$T\dot{s} = c_v \dot{T} - \left[ \frac{P}{\rho^2} - \left( \frac{\partial u}{\partial \rho} \right)_T \right] \dot{\rho} \quad (6)$$

where  $u$  is the internal energy and  $c_v$  is the heat capacity at constant volume. For the latter, we used the analytic fits of [Chabrier & Potekhin \(1998\)](#); [Potekhin & Chabrier \(2000\)](#). The heat capacity is calculated from the Helmholtz free energy assuming a fully ionized plasma consisting of point-like ions immersed in an electron background. The plasma is characterized by the Coulomb coupling parameter, defined as the ratio between the potential energy and the thermal energy:  $\Gamma = (Ze)^2 / (\kappa_B T a)$ , where  $a = (4\pi/3 n_i)^{-1/3}$  is the mean inter-ion distance and  $n_i$  is the ion number density. At  $\Gamma \lesssim 1$  the ions behave as a gas, at  $\Gamma > 1$  as a strongly coupled Coulomb liquid, while crystallization occurs at  $\Gamma = \Gamma_m \approx 175$ . The quantum effects are taken into account when  $T_p \ll \hbar\omega_p / \kappa_B$ , where  $\omega_p = (4\pi Z^2 e^2 n_i / m_i)^{1/2}$  is the ion plasma frequency.

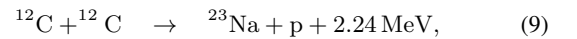
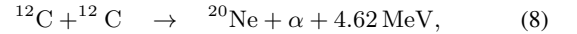
First, we integrate Eq. (5) with Eq. (6) neglecting the nuclear burning and neutrino emission processes. Fig. 8 shows the evolution of the WD central temperature for constant mass sequences ( $M_{\text{WD}} = 1.39, 1.42$  and  $1.46 M_{\odot}$ ) with two different initial temperature:  $T(0) = 10^7$  K and  $T(0) = 10^8$  K, respectively. They were obtained by solving simultaneously Eq. (2) and:

$$dT = \frac{P}{c_v(\rho, T)\rho} \frac{\partial \log \rho}{\partial J} dJ. \quad (7)$$

For the magnetic field evolution, we have adopted the two cases of the previous section: constant surface magnetic field (see Eq. (3)) and constant magnetic flux (see Eq. (4)) with  $B_0 = 10^6$  G. It is obvious that independently of the initial temperature, the WD configuration heats while it is compressing, as it is seen in Fig. 8.

In particular case, when  $T(0) = 10^7$  K (left panel of Fig. 8), there is a phase transition from solid to liquid state while the system is heating. This could change the thermal evolution due to the latent heat and will depend on the abundance of chemical species (see e.g. [Isern et al. 1997](#); [Chabrier 1997](#)). However, when  $T(0) = 10^8$  K (right panel of Fig. 8), the configuration of the WD has a Coulomb parameter  $\Gamma < 175$ , i.e. the matter is in liquid state along its entire evolution.

In order to introduce the nuclear burning and the neutrinos emission process we have considered that for the rotating  $^{12}\text{C}$  WDs the thermonuclear energy is essentially released by two nuclear reactions:



with nearly the same probability. For the carbon fusion reaction rate, we used the fits obtained by [Gasques et al. \(2005\)](#) and for the neutrino energy losses we used the analytical fits calculated by [Itoh et al. \(1996\)](#), which account for the electron-positron pair annihilation ( $e^- e^+ \rightarrow \nu \bar{\nu}$ ), photo-neutrino emission ( $e + \gamma \rightarrow e \nu \bar{\nu}$ ), plasmon decay ( $\gamma \rightarrow \nu \bar{\nu}$ ), and electron-nucleus bremsstrahlung [ $e(Z, A) \rightarrow e(Z, A) \nu \bar{\nu}$ ].

The central temperature evolution is shown in Fig. 9 when the carbon fusion energy release and the neutrinos energy losses are taken into account. This was done solving:

$$dT = \frac{P}{c_v(\rho, T)\rho} \frac{\partial \log \rho}{\partial J} dJ + \frac{\epsilon_{\text{nuc}} - \epsilon_{\nu}}{c_v(\rho, T)} dt \quad (10)$$

At the beginning, when  $T(0) = 10^7$  K, the configuration heats via the energy release from the carbon fusion and the compression of the configuration. However, when  $T(0) = 10^8$  K, the energy losses from the neutrino emission process is the dominant process and it cools the configurations.

Fig. 10 shows the evolutionary path of some constant mass sequences in the central temperature and central density plane. Fig. 10 shows also the lines where the neutrino emissivity equals the nuclear energy release (i.e. carbon-ignition line:  $\epsilon_{\text{nuc}} = \epsilon_{\nu}$ ) and the lines along which the characteristic time of nuclear reactions,  $\tau_{\text{nuc}}$ , equals 1 second and equals the dynamical timescale,  $\tau_{\text{dyn}}$ .

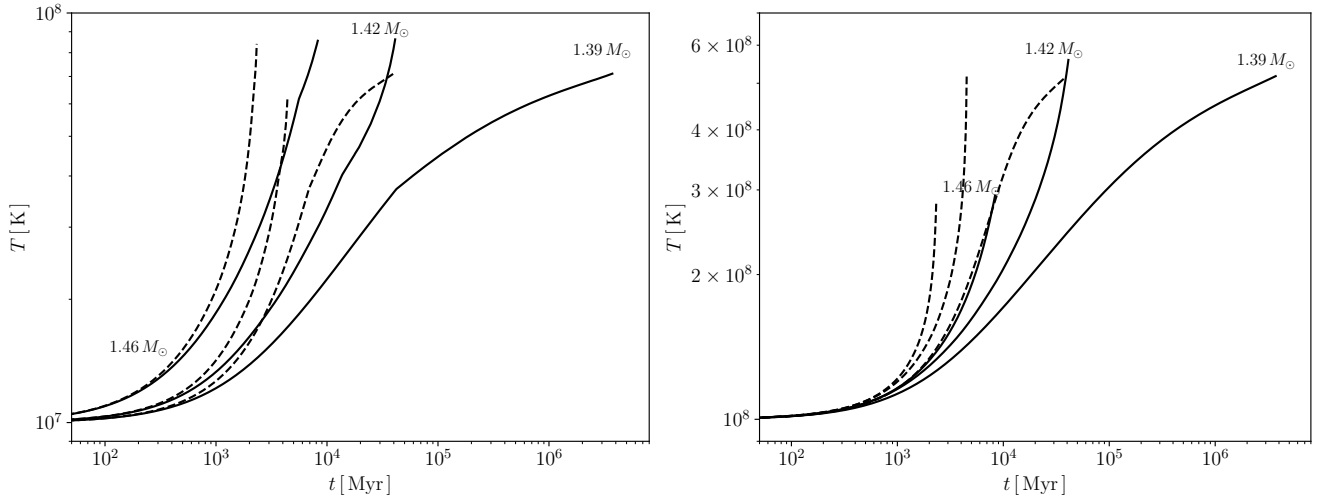


**Figure 8.** Central temperature versus time for constant mass sequences. The legend is the same as in Fig. 3. Left panel:  $T(0) = 10^7$  K. Right panel:  $T(0) = 10^8$  K.

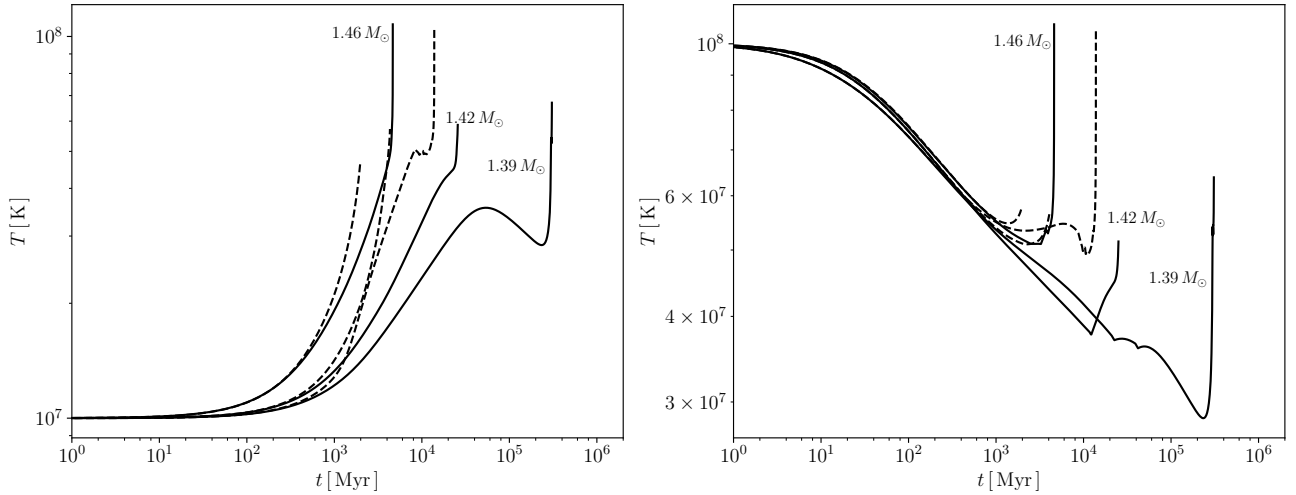


**Figure 9.** Central temperature versus time introducing carbon fusion energy release and neutrino energy losses. The legend is the same as in Fig. 3. Left panel:  $T(0) = 10^7$  K. Right panel:  $T(0) = 10^8$  K.

The dynamical timescale  $\tau_{\text{dyn}}$  is defined as:

$$\tau_{\text{dyn}} = \frac{1}{\sqrt{24\pi G\rho}}, \quad (11)$$

and the characteristic time of nuclear reactions is:

$$\tau_{\text{nuc}} = \frac{\epsilon_{\text{nuc}}}{\dot{\epsilon}_{\text{nuc}}} = c_p \left( \frac{\partial \epsilon_{\text{nuc}}}{\partial T} \right)^{-1} \quad (12)$$

As seen in Fig. 10, all the configurations cross the carbon-ignition line. When this happens, the star will be heated evolving to a state at which the fusion reactions becomes instantaneously ( $\tau_{\text{nuc}} < \tau_{\text{dyn}}$ ), possibly leading to a supernova. For some constant mass sequence, the configuration crosses the crystallization line, labeled as  $\Gamma = 175$  in Fig. 10. When  $T(0) = 10^8$  K, it happens just for  $M = 1.39 M_{\odot}$ , while for lower initial temperature it happens for all the constant mass sequence considered here.

In Tab. 1, we compare the time needed by the configuration to reach an instability limit (mass-shedding, secular axisymmetric instability and/or inverse  $\beta$  decay instability),  $\tau$  (see Eq. (1)), with the one needed to reach the carbon-ignition line when one just con-

siders the compression of the star,  $\Delta\tau_{\rho}$  (solving Eq. (7)), and when energy released from the carbon fusion and neutrino emission are introduced,  $\Delta\tau_{\text{CC}}$  (solving Eq. (10)), for the both magnetic field evolution: constant magnetic field and constant magnetic flux with  $B_0 = 10^6$  G.

We have also specified the mass of the configuration,  $M$ , the initial angular velocity,  $\Omega_0$ , the magnitude of the initial dynamical timescale,  $\tau_{\text{dyn},0}$  as well as the initial central temperature,  $T(0)$ . In all cases the star arrives first to the ignition line than to the instability limit. This time difference is greater for less massive WDs than for more massive WDs.

Finally, in Fig. 11, we show the  $\tau$ ,  $\Delta\tau_{\rho}$  and  $\Delta\tau_{\text{CC}}$  as a function of the surface magnetic field strength when the field intensity is assumed to be constant along all the evolution, for different constant mass sequences and different initial temperature. The stronger surface magnetic field the shorter the WD lifetime.

**Table 1.** Total WD Time Evolution ( $B_0 = 10^6$  G): the first four columns correspond to the WD total mass,  $M$ , WD initial angular velocity,  $\Omega_0$ , initial dynamical timescale,  $\tau_{\text{dyn},0}$  and initial central temperature,  $T(0)$ . The next three columns correspond to the time needed by the WD to reach an instability limit,  $\tau$  and to reach the carbon-ignition line when it just considers the compression of the star,  $\Delta\tau_\rho$ , and when energy released from the carbon fusion and neutrino emission are introduced,  $\Delta\tau_{\text{CC}}$ . First when the surface magnetic field is constant and then when the magnetic flux is constant.

				Constant Magnetic field			Constant Magnetic Flux		
$M$ $M_\odot$	$\Omega_0$ $\text{s}^{-1}$	$\tau_{\text{dyn},0}$ $10^{-4}$ s	$T(0)$ K	$\tau$ Myr	$\Delta\tau_\rho$ Myr	$\Delta\tau_{\text{CC}}$ Myr	$\tau$ Myr	$\Delta\tau_\rho$ Myr	$\Delta\tau_{\text{CC}}$ Myr
1.39	1.59	7.07	$10^8$	$3.76 \times 10^6$	$3.68 \times 10^4$	$2.64 \times 10^5$	$3.99 \times 10^4$	$6.54 \times 10^3$	$1.31 \times 10^4$
			$10^7$		$3.09 \times 10^5$	$2.64 \times 10^5$		$1.35 \times 10^4$	$1.31 \times 10^4$
			$10^6$		$3.13 \times 10^5$	$2.64 \times 10^5$		$3.54 \times 10^4$	$1.31 \times 10^4$
1.42	1.94	42.4	$10^8$	$4.28 \times 10^4$	$1.12 \times 10^4$	$2.53 \times 10^4$	$4.59 \times 10^3$	$3.46 \times 10^3$	$4.28 \times 10^3$
			$10^7$		$2.54 \times 10^4$	$2.53 \times 10^4$		$4.31 \times 10^3$	$4.28 \times 10^3$
			$10^6$		$2.57 \times 10^4$	$2.53 \times 10^4$		$3.99 \times 10^3$	$4.28 \times 10^3$
1.46	3.06	13.5	$10^8$	$8.51 \times 10^3$	$2.83 \times 10^3$	$4.39 \times 10^3$	$2.37 \times 10^3$	$1.91 \times 10^3$	$2.03 \times 10^3$
			$10^7$		$2.34 \times 10^3$	$4.45 \times 10^3$		$2.24 \times 10^3$	$2.03 \times 10^3$
			$10^6$		$4.53 \times 10^3$	$4.45 \times 10^3$		$2.03 \times 10^3$	$2.03 \times 10^3$

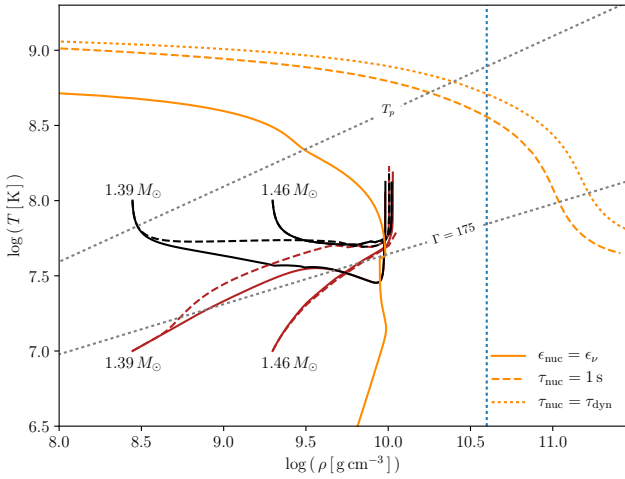


**Figure 10.** (Color online) Track evolution in the central density and central temperature plane with carbon fusion energy release and neutrino energy losses. We also show the carbon-ignition line (solid orange line), the line along which  $\tau_{\text{nuc}} = 1$  s and  $\tau_{\text{nuc}} = \tau_{\text{dyn}}$ , the crystallization line labeled as  $\Gamma = 175$ , and the plasma temperature line defined as  $\kappa_B T_p = \hbar\omega_p$ .

## 6 CONCLUDING REMARKS

We have investigated in this work the evolution of the WD structure while it loses angular momentum via magnetic dipole braking. We obtained the following conclusions:

(i) We have computed the lifetime of SCWDs as the total time it spends in reaching one of the following possible instabilities: mass-shedding, secular axisymmetric instability and inverse  $\beta$  decay instability. The lifetime is inversely proportional both to the magnetic field and to the mass of the WD (see Fig. 4).

(ii) We showed how the parameters of rotating WDs evolve with time. For the sake of comparison we considered two cases: a constant magnetic field and a varying magnetic field conserving magnetic flux. We showed that the WD is compressed with time. It turns out that, in the case of magnetic flux conservation, the evolution times are shorter than for the constant magnetic field, hence the WD lifetime.

(iii) The time scales of Ilkov & Soker (2012); Külebi et al.

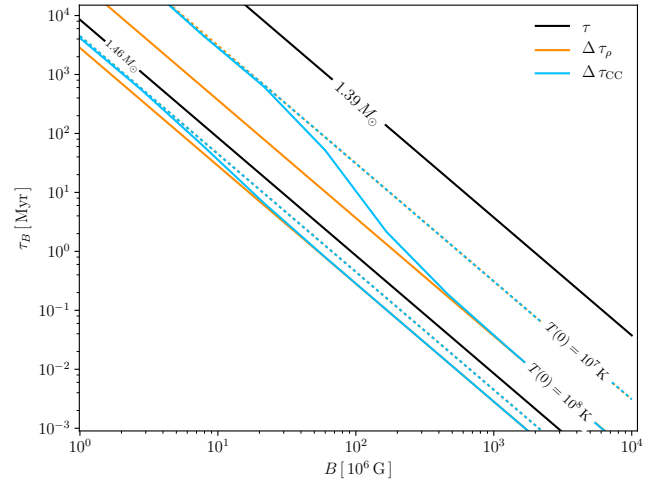


**Figure 11.** (Color online) Characteristic times of the WD evolution as a function of the surface magnetic field. Here, it is compared with the total time needed by the WD configuration to reach an instability limit,  $\tau$  (solid black lines), the one needed to reach the carbon-ignition line when one just considers the compression of the star,  $\Delta\tau_\rho$  (orange lines), and when energy released from the carbon fusion and neutrino emission are introduced,  $\Delta\tau_{\text{CC}}$  (blue lines).

(2013) are consistent with the ones in Fig. 4 only for the maximum mass value  $M/M_{\text{max}}^{J=0} \approx 1.06$ .

(iv) Whether or not the SCWD can end its evolution as a type Ia supernova as assumed e.g. by Ilkov & Soker (2012) is a question that deserves to be further explored. Here, we have computed the evolution of the WD central temperature while it loses angular momentum along constant mass sequence. In general, the WD will increase its temperature while it is compressed. When carbon fusion reaction and neutrino emission cooling are considered, the evolution depends on the initial temperature. However, in all the cases studied, the configurations reach the carbon-ignition line. In this point the speed of the carbon fusion reactions increases until reaching conditions for a thermonuclear explosion.

(v) We have also computed the time that the SCWDs need in reaching the carbon-ignition line (central temperature and density conditions at which the energy release from the carbon fusion re-

actions equals the neutrino emissivity). This time is shorter than the timescale needed by the WD to reach mass-shedding, secular axisymmetric instability and/or inverse  $\beta$  decay instability.

(vi) If a magnetized sub-Chandrasekhar WD has a mass which is not very close to the non-rotating Chandrasekhar mass, then it evolves slowing down and on a much longer time scales with respect to SCWDs. It gives us the possibility to observe them during their life as active pulsars. Soft gamma-repeaters and anomalous X-ray pulsars appear to be an exciting possibility to confirm such a hypothesis (Malheiro et al. 2012; Boshkayev et al. 2013a; Rueda et al. 2013). The massive, highly magnetized WDs produced by WD binary mergers, recently introduced as a new class of low-luminosity gamma-ray bursts (Rueda et al. 2018b,a) would be another interesting case.

(vii) A magnetized WD produced in a WD binary merger will be surrounded by a Keplerian disk (García-Berro et al. 2012). Thus, to compute its evolution we have to consider the star-disk coupling and the angular momentum transfer from the disk to the WD (Rueda et al. 2013). This new ingredients would appear to invalidate our assumption of an isolated WD and the general picture draw in this work. However, as shown by Rueda et al. (2013), accretion from the disk occurs in very short time scales and the WD lives most of its evolution in the dipole magnetic braking phase. Thus, we expect the WD lifetime computed in this work to be a good estimate also for those systems. In that case it is important to estimate the lifetime for the final WD mass after the accretion process since, as we have shown in Fig. 4, even a small increase in mass shortens drastically the lifetime.

## ACKNOWLEDGEMENT

The work was supported in part by Nazarbayev University Faculty Development Competitive Research Grants: 'Quantum gravity from outer space and the search for new extreme astrophysical phenomena', Grant No. 090118FD5348 and by the MES of the RK, Program 'Center of Excellence for Fundamental and Applied Physics' IRN: BR05236454, and by the MES Program IRN: BR05236494.

## REFERENCES

- Boshkayev K., Rueda J., Ruffini R., 2011, *International Journal of Modern Physics E*, **20**, 136
- Boshkayev K., Izzo L., Rueda Hernandez J. A., Ruffini R., 2013a, *A&A*, **555**, A151
- Boshkayev K., Rueda J. A., Ruffini R., Siutsou I., 2013b, *ApJ*, **762**, 117
- Boshkayev K., Rueda J., Ruffini R., 2014a, *International Journal of Mathematics and Physics*, **5**, 33
- Boshkayev K., Rueda J. A., Ruffini R., Siutsou I., 2014b, *Journal of Korean Physical Society*, **65**, 855
- Boshkayev K., Rueda J. A., Ruffini R., 2015a, in Rosquist K., ed., Thirteenth Marcel Grossmann Meeting On General Relativity. pp 2295–2300 ([arXiv:1503.04176](https://arxiv.org/abs/1503.04176)), doi:10.1142/9789814623995\_0424
- Boshkayev K., Rueda J. A., Ruffini R., Siutsou I., 2015b, in Rosquist K., ed., Thirteenth Marcel Grossmann Meeting On General Relativity. pp 2468–2474 ([arXiv:1503.04171](https://arxiv.org/abs/1503.04171)), doi:10.1142/9789814623995\_0472
- Boshkayev K., Rueda J. A., Ruffini R., Zhami B., 2017, in Jantzen R., ed., Fourteenth Marcel Grossmann Meeting On General Relativity. pp 4379–4384 ([arXiv:1604.02393](https://arxiv.org/abs/1604.02393))
- Chabrier G., 1997, in Bedding T. R., Booth A. J., Davis J., eds, IAU Symposium Vol. 189, IAU Symposium. pp 381–388 ([arXiv:astro-ph/9705062](https://arxiv.org/abs/astro-ph/9705062))
- Chabrier G., Potekhin A. Y., 1998, *Phys. Rev. E*, **58**, 4941
- Chandrasekhar S., 1931, *ApJ*, **74**, 81
- García-Berro E., et al., 2012, *ApJ*, **749**, 25
- Gasques L. R., Afanasjev A. V., Aguilera E. F., Beard M., Chamon L. C., Ring P., Wiescher M., Yakovlev D. G., 2005, *Phys. Rev. C*, **72**, 025806
- Geroyannis V. S., Papatotiriou P. J., 2000, *ApJ*, **534**, 359
- Hartle J. B., 1967, *ApJ*, **150**, 1005
- Iben Jr. I., Tutukov A. V., 1984, *ApJS*, **54**, 335
- Ilkov M., Soker N., 2012, *MNRAS*, **419**, 1695
- Isern J., Mochkovitch R., García-Berro E., Hernanz M., 1997, *ApJ*, **485**, 308
- Itoh N., Hayashi H., Nishikawa A., Kohyama Y., 1996, *ApJS*, **102**, 411
- Kepler S. O., et al., 2015, *MNRAS*, **446**, 4078
- Kilic M., Hambly N. C., Bergeron P., Genest-Beaulieu C., Rowell N., 2018, *MNRAS*, **479**, L113
- Külebi B., Ekşi K. Y., Lorén-Aguilar P., Isern J., García-Berro E., 2013, *MNRAS*, **431**, 2778
- Malheiro M., Rueda J. A., Ruffini R., 2012, *PASJ*, **64**, 56
- Potekhin A. Y., Chabrier G., 2000, *Phys. Rev. E*, **62**, 8554
- Rotondo M., Rueda J. A., Ruffini R., Xue S.-S., 2011a, *Phys. Rev. C*, **83**, 045805
- Rotondo M., Rueda J. A., Ruffini R., Xue S.-S., 2011b, *Phys. Rev. D*, **84**, 084007
- Rueda J. A., Boshkayev K., Izzo L., Ruffini R., Lorén-Aguilar P., Külebi B., Aznar-Siguán G., García-Berro E., 2013, *ApJ*, **772**, L24
- Rueda J. A., et al., 2018a, *arXiv e-prints*,
- Rueda J. A., et al., 2018b, *J. Cosmology Astropart. Phys.*, **10**, 006
- Salpeter E. E., 1961, *ApJ*, **134**, 669
- Shapiro S. L., Teukolsky S. A., 1983, *Black holes, white dwarfs, and neutron stars: The physics of compact objects*. New York, Wiley-Interscience
- Shapiro S. L., Teukolsky S. A., Nakamura T., 1990, *ApJ*, **357**, L17
- Webbink R. F., 1984, *ApJ*, **277**, 355